NANO LETTERS

2007
Vol. 7, No. 6
1770−1778

Wetting Driven Self-Assembly as a New Approach to Template-Guided Fabrication of Metal Nanopatterns

Devasish Chowdhury, Rivka Maoz, and Jacob Sagiv*

Department of Materials and Interfaces, The Weizmann Institute of Science, Rehovot 76100, Israel

Received April 10, 2007; Revised Manuscript Received May 3, 2007

ABSTRACT

Wetting driven self-assembly (WDSA) of appropriate materials in their liquid state on organic monolayer nanopatterns consisting of wettable (lyophilic) surface features surrounded by a nonwettable (lyophobic) monolayer background is shown to provide the basis of a versatile new approach to template-guided fabrication of metal nanopatterns. Monolayer nanopatterns with planned distributions of lyophilic/lyophobic surface regions are conveniently generated by *constructive nanolithography* upon local electrochemical oxidation of the top –CH_3 groups of a highly ordered OTS (*n*-octadecyltrichlorosilane) monolayer self-assembled on silicon to –COOH (*Adv. Mater.* 2000, *12*, 725–731). Retraction of such a patterned monolayer from a liquid that does not wet its nonpolar –CH_3 surface (lyophobic) results in selective, site-defined immobilization of nanosized volumes of the liquid on the locally generated polar –COOH groups (lyophilic). Examples are given of WDSA of organic materials that offer further options for post-assembly chemical processing, such as nonvolatile low-melting olefins, acids, or thiols, the former being in situ reacted to generate polar functions like –COOH or –SH. Loading surface patterns created in this manner with silver or gold ions followed by further chemical processing results in elemental metal nanoparticles generated within the ion-binding organic material, which thus functions as a guiding template for planned metal deposition at predefined surface sites. WDSA is particularly versatile, as any nonvolatile material with appropriate melting temperature and surface wetting characteristics or solubility in a liquid displaying such properties may in principle be utilized to fabricate potentially useful surface nanostructures.

Wetting driven self-assembly (WDSA) is a template-guided self-assembly strategy that offers a simple and straightforward means for the fabrication of surface immobilized nanostructures by taking advantage of the selective adhesion of nanosized volumes of wetting liquids to the lyophilic surface regions of heterogeneous lyophilic/lyophobic surface nanopatterns. It has been shown that such nanopatterns displaying high lyophilic/lyophobic contrast can by generated by local electrochemical oxidation of the top $-CH_3$ groups of a highly ordered OTS (*n*-octadecyltrichlorosilane) monolayer self-assembled on silicon to −COOH.[1] The patterning process is carried out with the help of an electrically biased SFM (scanning force microscope) tip operated as a writing pen, under conditions that preserve the basic structural integrity of the patterned monolayer.[1,2] This paved the way to the advancement of *constructive nanolithography* (CN), a generic bottom-up assembly strategy that utilizes nondestructively patterned organosilane monolayers as templates in diverse post-patterning chemical processes designed to further develop the initially inscribed surface information.[1,3−8] For example, we have demonstrated the feasibility of several template-guided hierarchical self-assembly routes, starting with the site-selective self-assembly of an organized top monolayer of NTS (18-nonadecenyltrichlorosilane, $CH_2{=}CH{-}(CH_2)_{17}{-}SiCl_3$) on the tip-inscribed sites[1,4,5,7] of a patterned OTS monolayer. The terminal ethylenic groups of NTS can be chemically modified so as to generate various functional template patterns as elevated copies of the base monolayer pattern on which NTS was assembled. Bilayer/monolayer template patterns produced in this manner have been used to control the subsequent in situ surface generation of CdS,[1,4] silver,[1,4,9] and gold,[4,9] as well as the anchoring at predefined surface sites of ex situ synthesized species like [Au55] clusters[5] and colloidal gold nanoparticles.[7]

The CN strategy based on site-selective self-assembly of monolayer-forming compounds like NTS allows the formation of well-defined nanopatterned templates, equipped with various desired chemical functions. Self-assembled organosilane mono- and multilayers are remarkably robust surface entities, capable of withstanding rather harsh thermal conditions[10] and chemical modification operations[11−17] with full preservation of their high molecular order and structural integrity. The inherent subnanometric precision set by the well-defined molecular size and 3D organization of such systems[14−17] offers important advantages in terms of the ultimate resolution, stability, and reproducibility achievable

* Corresponding author. E-mail: jacob.sagiv@weizmann.ac.il. Telephone: +972-8-9342309. Fax: +972-8-9344138.

10.1021/nl070842x CCC: $37.00
Published on Web 05/22/2007

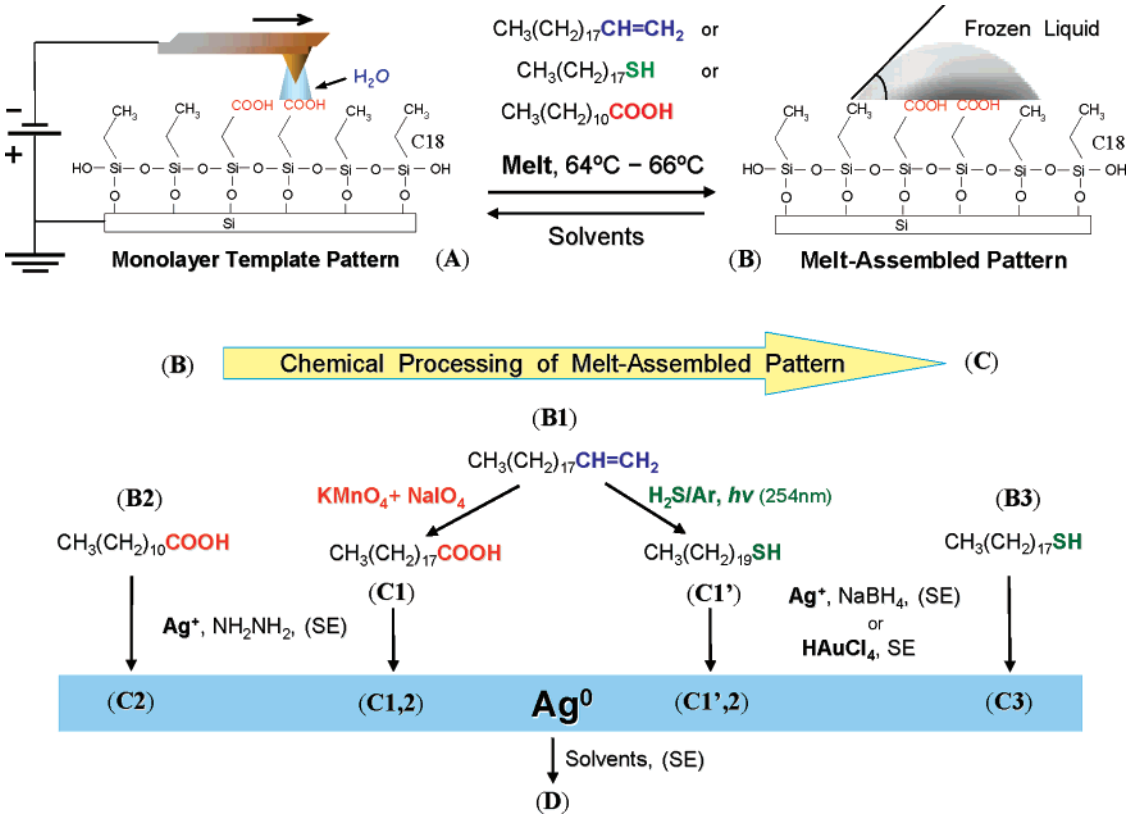

Figure 1. Schematic illustration of WDSA@CN as a generic approach to template-guided fabrication of surface-immobilized metal nanopatterns. Several examples of possible fabrication pathways are indicated, starting with (A) the nanoelectrochemical (SFM tip-assisted) patterning of a highly ordered OTS monolayer self-assembled on silicon[1] and (A → B) the subsequent selective immobilization of a selected organic material from its melt (e.g., eicosene, octadecanethiol, dodecanoic acid) on the lyophilic (−COOH) sites of the monolayer pattern thus created. (B → C) In situ chemical modifications of the melt-assembled patterns (after solidification at the ambient temperature), designed to lead to the generation of various metal−organic hybrid nanostructures: (B1 → C1) oxidation of the terminal ethylenic group of eicosene (B1) with aqueous $KMnO_4$ + $NaIO_4$ (30 min, pH = 8.5, room temp)[1,26] yields nonadecanoic acid (C1), and (B1 → C1′) gas-phase photoreaction with H_2S/Ar (λ = 254 nm, 10 min, room temp)[1,3−5] yields eicosanethiol (C1′). Site-defined generation of metallic silver may be achieved via a number of different template-controlled processes. The options indicated here are: (C1 → C1,2; B2 → C2) binding of Ag^+ ions (upon treatment for 2 min with an aqueous solution of silver acetate) to the carboxylic acid groups of the nonadecanoic acid (C1) or dodecanoic acid (B2),[4,27] or (C1′ → C1′,2; B3 → C3) to the thiol groups of eicosanethiol (C1′) or octadecanethiol (B3),[1,3,9,27] followed by subsequent reduction to elemental silver (Ag^0), upon exposure (for 10 min) to respectively gaseous N_2H_4[4,27] or aqueous $NaBH_4$.[1,3,9,27] Optional further development of initially generated metal nanoparticles may be achieved by treatment with a silver enhancer (SE) solution.[1,3,4,27] The spontaneous reduction of Au^{3+} species to elemental gold upon reactive binding of $HAuCl_4$ to eicosanethiol (C1′) or octadecanethiol (B3)[28] may also be used to catalyze silver metal deposition from the SE solution (C1′ → C1′,2; B3 → C3). (D) Finally, selective removal of soluble organic material from each of the metal−organic hybrid structures generated in processes B → C is possible upon immersion (for 30 min) in suitable organic solvents (dodecanoic and nonadecanoic acids in chloroform, octadecanethiol and eicosanethiol in diethyl ether), as well as optional further growth (upon treatment with the SE solution) of the metal features left on the surface. Note the reversibility of the assembly process A ↔ B, as melt-assembled patterns of these materials can be easily "erased" by dissolution in a suitable solvent, thus regenerating the respective monolayer template patterns.

in the bottom-up fabrication of complex supramolecular surface architectures. However, the use of purpose-designed monolayer-forming compounds is subject to their limited availability, as the preparation of such special molecular building blocks may involve complex and costly synthetic protocols.[11,17−21] Another limitation has to do with the irreversible anchoring of molecules like NTS to an initially generated monolayer pattern. While conferring high stability, this has the undesirable consequence of not allowing the repeated use of a base monolayer pattern in different post-patterning assembly processes, which would offer a flexible and versatile research tool. WDSA was thus explored from the perspective of possible broadening of the scope of constructive nanolithography as a generic bottom-up approach to nanofabrication. Although lacking some of the desirable features of precise molecular self-assembly, it was anticipated that this approach might offer attractive new options for in situ chemical synthesis in "nanoreactors" confined at predefined sites on a solid surface.

In this communication, we briefly report results obtained in a series of proof-of-concept experiments (Figure 1) conducted with three model organic compounds, selected on the basis of the following combination of desirable properties: nonvolatile solids with low melting points above the ambient temperature, surface tensions (in the melted state) that should allow complete wetting by the liquid (zero contact angle) of lyophilic surfaces rich in polar groups such as −COOH while preventing adhesion (sufficiently high contact angles) to the lyophobic $-CH_3$ surface of a highly ordered OTS monolayer, molecular structures allowing straightfor-

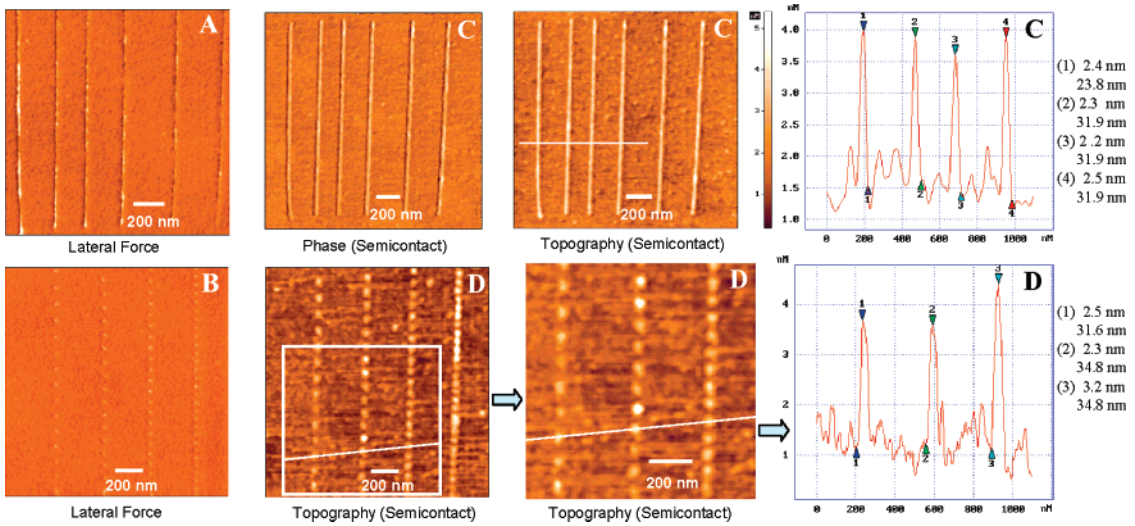

Figure 2. Eicosene nanopatterns assembled from the melt as indicated in Figure 1. (A,B) Lateral force (friction) contact mode SFM images of monolayer template lines and dot-lines patterns corresponding to step A in Figure 1. (C) From left to right: phase and simultaneously recorded topographic semicontact mode SFM images of melt-assembled eicosene nanowires formed on the monolayer template pattern shown in A (step B in Figure 1), and distance−height profile along the marked line in the respective topographic image. (D) Topographic images (as in C) of melt-assembled eicosene dot-lines formed on the monolayer template pattern shown in B, and distance−height profile along the marked line in the respective topographic images (the right side image shows a detailed scan of the marked area in the left side image). Both patterns were produced on same silicon wafer substrate, with the eicosene assembly occurring simultaneously on the continuous lines and the dot-lines. The pattern inscription (A,B) was done with a Solver P47 instrument (NT-MDT, Moscow, Russia) operated in the spectroscopic mode provided by the instrument software (400 spectroscopic scanned points/patterned area), using doped (uncoated) μMasch silicon probes with spring constants of 0.01−0.08 N/m operated under a controlled humidity atmosphere (~65% relative humidity), to which a negative tip bias of 8.0−8.2 V[29] relative to the surface was applied. Contact mode images were obtained in the ambient atmosphere (with the probe used for patterning without electrical bias and minimal contact force) immediately after the inscription of the respective monolayer patterns. Semicontact mode images were acquired with the same instrument using Olympus probes (AC 160 TS) with spring constant of 42 N/m and resonance frequency of 300 kHz.

ward infrared spectroscopic characterization by comparison with long-tail amphiphilic compounds routinely employed in monolayer self-assembly, not expensive and readily available.[22−25] It was further anticipated that nanopatterns made of compounds equipped with functional groups exhibiting affinity for noble metal ions might become useful as organic templates in processes of post-assembly chemical generation of metal nanopatterns. As indicated in Figure 1, the three long-tail hydrocarbon derivatives selected for this study, eicosene ($CH_3-(CH_2)_{17}-CH=CH_2$), octadecanethiol ($CH_3-(CH_2)_{17}-SH$), and dodecanoic acid ($CH_3-(CH_2)_{10}-COOH$), allowed us to evaluate both certain basic aspects of the WDSA at nanoscale dimensions[22−25] and the feasibility of a number of different post-assembly chemical processing routes conducive to the formation of planned metal nanopatterns.

Planned patterns of each of the three selected compounds were generated by slow retraction of silicon wafer substrates bearing the desired tip-inscribed monolayer template patterns from the respective melts (process A → B in Figure 1). It was found that assembly experiments carried out around 64−66 °C (i.e., more than 35 °C above the melting points of eicosene and octadecanethiol and 20 °C above that of lauric acid), with substrates being pulled out from the liquid at the lowest speed provided by a motor-driven lift used for this purpose (around 66−67 μm/s),[22,23] gave optimal results in terms of the wetting/nonwetting selectivity of material deposition. Under these conditions, melt-assembled patterns with practically no traces liquid sticking to the lyophobic OTS surface could be routinely produced. Because eicosene melts around 28−29 °C, octadecanethiol around 30 °C, and lauric acid around 44 °C, surface patterns assembled from such melts solidify upon withdrawal of the substrate from the respective liquid phases into the ambient (22° ± 1 °C, in our laboratory). This greatly facilitates both their SFM imaging and post-assembly chemical processing. Various post-assembly chemical modification sequences could thus be carried out without removal from the surface of the deposited organic material or the in situ generated metal particles by using aqueous or gas-phase reagents and taking advantage of selective solubilities of different chemical species in different solvents (processes B → C → D in Figure 1).

Examples of melt-assembled eicosene nanopatterns produced by the present process are shown in Figure 2. The writing of the monolayer template patterns in all experiments reported here was done with sharp silicon probes (doped, uncoated), which turned out to be sufficiently conductive for this purpose[29] and thus allowed inscription of smaller features (down to ~6 nm) compared to those usually produced with blunter probes bearing conductive coatings.[1−8] As reported before, the features inscribed on the OTS monolayer display higher friction compared to the surrounding OTS background (Figure 2A,B), associated with the local conversion of the nonpolar $-CH_3$ to polar −COOH groups, while only a weak negative contrast is visible in the corresponding topographic images (not shown).[2,7]

Eicosene is seen to assemble selectively on the tip-inscribed monolayer sites, yielding features that are clearly

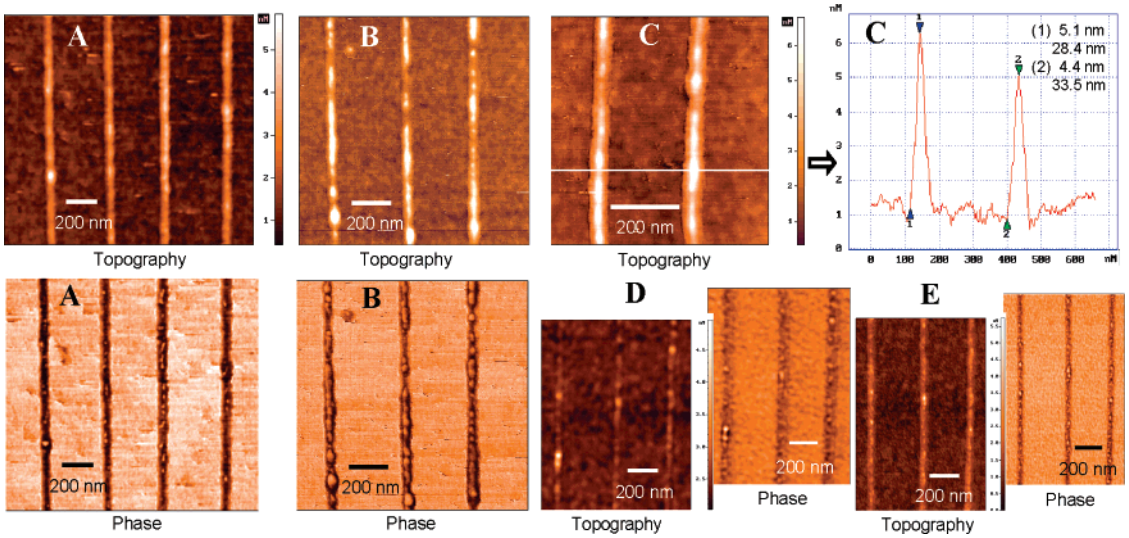

Figure 3. Semicontact mode SFM topographic and simultaneously recorded phase images (acquired as in Figure 2) of chemically modified eicosene nanowires taken at each step along chemical modification path B1 → C1→ C1,2 → D indicated in Figure 1. (A) After in situ conversion of eicosene to nonadecanoic acid (C1 in Figure 1). (B) A portion of the pattern shown in A after generation of elemental silver within the nonadecanoic acid template (C1,2 in Figure 1). (C) As B, showing a detailed scan of a portion of the Ag^0−nonadecanoic acid hybrid pattern, and distance−height profile along the marked line. (D) Images taken after dissolution in chloroform of the nonadecanoic acid from the hybrid metal−organic nanowires shown in B. (E) same nanowires as in D, after mild development of the silver nanoparticles with the SE solution (D in Figure 1).

visible both in the topographic and corresponding phase images (Figure 2C,D). Although these melt-assembled patterns are remarkably robust, resisting Scotch tape peeling as well as SFM imaging in the contact mode, to avoid possible mechanical damage, most images were acquired in the semicontact mode. The height values derived from the topographic images (Figure 2C,D), 2.6 ± 0.3 nm (wires) and 2.7 ± 0.6 nm (dots), are consistent with the expected thickness of an ordered monolayer of eicosene molecules (densely packed 20-carbon-atom chains in their fully extended all-*trans* conformation) oriented normal to the surface.[15,16,30] The uniform and continuous appearance of both the wires and the dots would further suggest that the solidified material resembles an amorphous supercooled liquid rather than a bulk polycrystalline phase. One may thus speculate that eicosene, like similar nonamphiphilic long-chain *n*-alkanes, adopts under the present surface assembly conditions the rotator phase structure of a monolayer with molecules oriented normal to the surface.[30] Infrared spectral data obtained from ultrathin films of eicosene similarly produced by retraction from the melt on large unpatterned surfaces coated with a carboxylic acid-terminated base monolayer (vide infra) are also consistent with this possible interpretation.[31]

There are significant differences between the apparent lateral dimensions of each individual eicosene feature (widths of ca. 28 ± 4 nm for the wires and ca. 31 ± 4 nm for the dots) and those of the corresponding tip-inscribed monolayer template features (respectively 11 ± 2.5 nm and 12.5 ± 5 nm), as determined from the lateral force images (compare parts A and B, respectively, with parts C and D of Figure 2). Part of this broadening may have to do with artifactal effects of the SFM imaging,[7] however, much of it appears to be real considering the fact that height variations between ca. 1.0 and ca. 5.5 nm, associated with the various chemical modifications of the initial eicosene features, are not accompanied by corresponding large width variations that might be ascribed to convolution with the SFM tip (see Figure 3 below). These observations appear to confer experimental support to the theoretically predicted spillover of liquids retained on lyophilic surface domains of nanoscale dimensions surrounded by a lyophobic surface,[32] so that the actual area occupied by the liquid exceeds the boundary of the wettable domain to which the liquid adheres.[22]

The feasibility of the in situ chemical processing routes indicated in Figure 1 was checked in experiments conducted on both melt-assembled nanopatterns and ultrathin films (with thicknesses in the range of several monolayers) of the respective materials similarly produced on large unpatterned base monolayer surfaces. This enabled us to follow the various investigated processes by both SFM and quantitative infrared and UV−visible spectroscopic techniques. Examples of SFM images taken at different stages during the in situ chemical pocessing of melt-assembled nanopaterns of, respectively, eicosene and octadecanethiol are given in Figures 3 and 4. Figures 5 and 6 present examples of pertinent FTIR and UV−vis spectral data collected from large area film samples exposed to same chemical modification sequences as the corresponding nanopatterns. The spectroscopic data provide direct evidence for the virtually quantitative transformations effected by each of the indicated chemical operations as well as for the overall structural stability of the film assemblies undergoing the respective transformations (vide infra). These findings are essential for a proper interpretation of the SFM images in Figures 3 and 4.

Unlike the rather continuous appearance of the initial eicosene nanowires (Figure 2C), the nonadecanoic acid

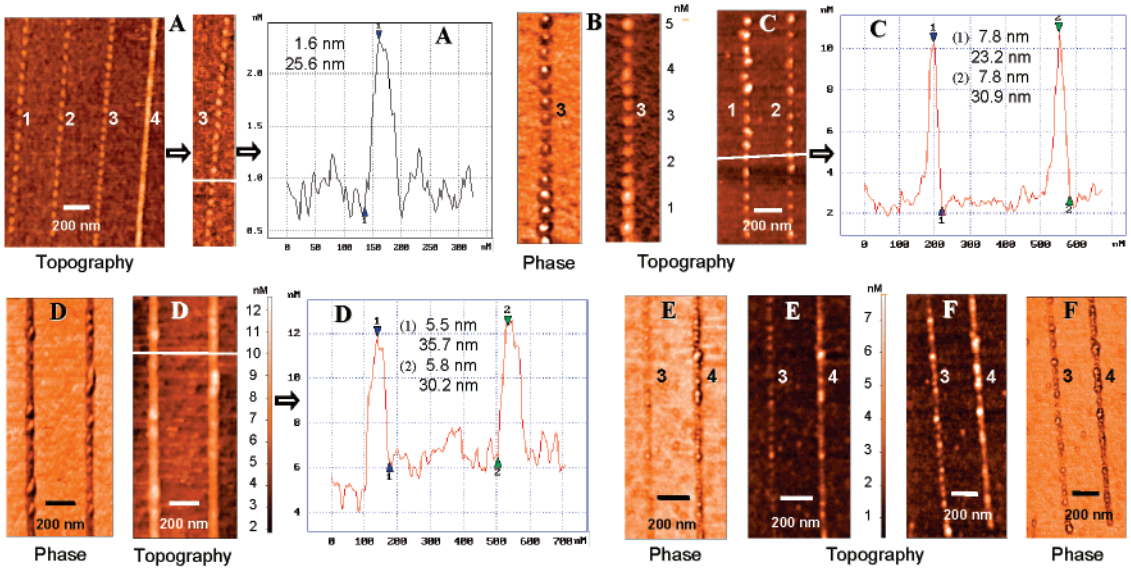

Figure 4. Semicontact mode SFM images as in Figures 2 and 3 showing examples of the evolution of melt-assembled octadecanethiol nanopatterns at various steps along chemical modification path B3 → C3 → D indicated in Figure 1. (A) Melt-assembled dot-lines with variable inter-dot spacing (B3 in Figure 1), and distance-height profile across the marked dot in the detailed scan image of a portion of dot-line no. 3. (B) Portion of dot-line no. 3 after generation of elemental silver via the $HAuCl_4$, SE process (B3 → C3 in Figure 1).[28] (C) Portion of dot-lines nos. 1 and 2 after the generation of elemental silver (as in B) followed by additional mild development of the silver nanoparticles with the SE solution (C3 in Figure 1), and distance−height profile along the line crossing two of the dots. (D) Portion of a pattern of nanowires (produced together with the dot-lines on the same silicon substrate) after generation of elemental silver (as in B), and distance−height profile along the marked line in the respective topographic image. (E) Portion of dot-lines nos. 3 and 4 after silver generation (as in C) followed by dissolution of the octadecanethiol in diethyl ether (note the apparently overlapping octadecanethiol dots in dot-line no. 4, image A). (F) same as (E), after further mild development of the silver nanoparticles with the SE solution (D in Figure 1).

resulting from the in situ oxidation of the eicosene is seen to cluster into particulate features aligned along each wire track (Figure 3A). This is consistent with the expected polycrystalline morphology of the polar acid derivative vis-à-vis the apparently amorphous nature of its nonpolar hydrocarbon precursor. Except for a growth in height of ca. 2−3 nm per particle, the general appearance of the wires after the generation of elemental silver resembles that of the nonadecanoic acid template (Figure 3B,C). According to the infrared and UV−vis data (vide infra), one would expect that each of these hybrid metal−organic nanoparticles consists of a metal core covered by a shell made of insoluble silver nonadecanoate and soluble nonadecanoic acid, generated upon the reduction of the silver nonadecanoate salt precursor to elemental silver and free acid. Treatment with chloroform is seen to drastically reduce the heights of the features left on the surface, from an average of 5.4 (±1.0) nm to 1.1 (±0.3) nm, while causing only a small relative decrease of their widths, from 31.5 (±5.0) nm to 28.0 (±7.0) nm (Figure 3D). Subsequent development with the silver enhancer solution adds, on the average, ca. 2 and 3 nm to their heights and widths, respectively (Figure 3E). This is unequivocal evidence for the metallic nature of the platelike features visible in Figure 3D, however, their small thickness is not compatible with the presence of an insoluble organic monolayer coating of the kind present on metal particles generated within the organic films (see IR and UV−vis data below).

Results of a different set of experiments, designed to check the generation of metallic silver within a melt-assembled template pattern made of a compound bearing a well-defined Ag^+-binding function are shown in Figure 4. The use of a commercially available functional compound such as octadecanethiol in the WDSA process circumvents the need of carrying out post-assembly chemical modification steps for the in situ installation of the desired metal ion binding function, which thus simplifies the overall fabrication process and avoids more complex situations arising from eventual incomplete conversions or the generation of more than a single reaction product.

The organization of melt-assembled octadecanethiol on both continuous monolayer template lines (not shown) and dot-lines (Figure 4A) resembles that of eicosene (Figure 2C,D), with similar wire heights (2.8 ± 0.4 nm) but lower dot heights (1.8 ± 0.3 nm). A similar lateral broadening relative to the respective tip-inscribed monolayer template features was observed as well, from ca. 15 ± 4 nm to 33 ± 6 nm, for the wires, and from ca. 11 ± 4 nm to 24 ± 2 nm for the dots. As in the case of the nonadecanoic acid, the generation of elemental silver within the octadecanethiol template was also expected to result in the formation of hybrid metal−organic nanoparticles, each consisting of a metal core covered by an insoluble coating of silver octadecanethiolate and a soluble octadecanethiol shell (see IR and UV−vis data below). However, unlike in the reduction of silver nonadecanoate, here elemental silver is generated by development (with the SE solution) of tiny gold clusters spontaneously formed upon the treatment of the thiol template with $HAuCl_4$.[28] It is thus possible to either grow metal particles up to the desired size in the presence of the organic material (Figure 4B,C) or, as done before (Figure 3D,E), after its removal (Figure 4E,F). The latter process is

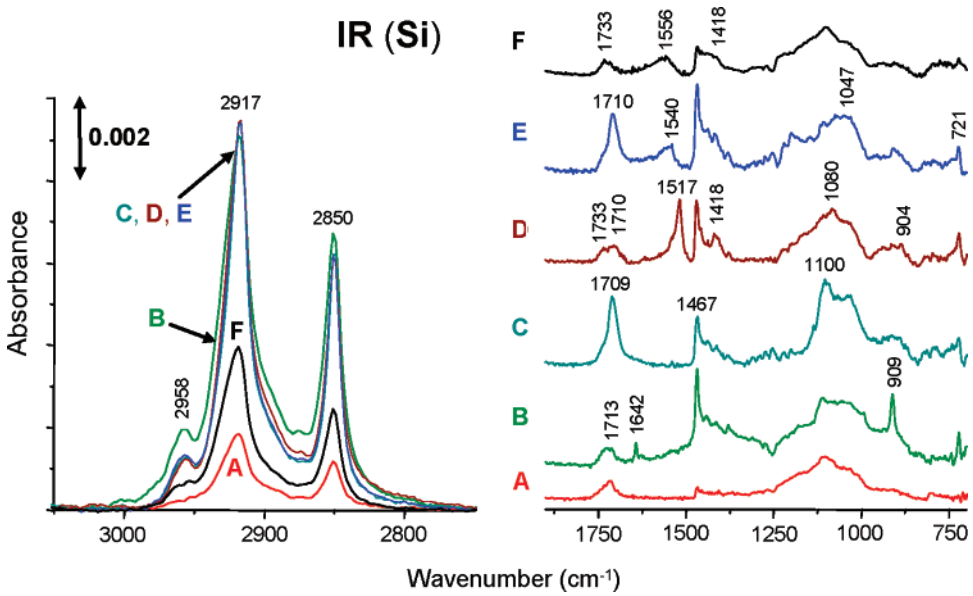

Figure 5. Quantitative Brewster angle FTIR (Fourier transform infrared) spectra[15,16,34] recorded at consecutive steps during the preparation and subsequent chemical processing (as indicated in Figure 1) of a thin film of eicosene assembled from melt on a base monolayer template with terminal −COOH functions produced on both sides of a double-side-polished silicon wafer (NTSox/Si) substrate (see text). (A) NTSox/Si base monolayer. (B) Eicosene thin film assembled on the NTSox/Si base monolayer (B1 in Figure 1). (C) Nonadecanoic acid film resulting from the exposure of B for 12 h to the $KMnO_4 + NaIO_4$ reagent (C1 in Figure 1). (D) Same film after conversion of nonadecanoic acid to its silver salt (upon 2 min treatment with 1.0×10^{-3} M aqueous silver acetate). (E) (D) after reduction of Ag^+ ions to elemental silver, upon 10 min exposure to gaseous hydrazine (C1,2 in Figure 1). (F) Same film after extraction of soluble organic material with chloroform (D in Figure 1). All curves represent net spectra of the respective film coatings, after subtraction of the spectral contributions of the bare silicon substrate.

of particular interest, as growth of the metal cores in the absence of a reservoir of organic shell molecules may be advantageous in the fabrication of conductive nanowires with intimate interparticle electrical contacts.

One may note that the fabrication of a continuous metal nanowire starting from a continuous organic nanowire template is not straightforward because of the observed metal coalescence occurring in the process of metal nucleation and growth, which disfavors the formation of elongated metal features with high aspect ratios (Figure 4D). In the case of sufficiently small nanodots, the same metal coalescence tendency effects the growth of a single metal core within each isolated template dot (Figure 4A−C). This led us to speculate that such template dot-lines with interdot separations comparable with the size of the dots themselves could offer a means for controlled assembly of lines of isolated but close-lying metal−organic nanoparticles, which, upon stripping of their organic shells and fine-tuning of their additional growth, might establish intimate contacts with one another and thus create continuous electrical conduction paths. The observed evolution of four dot-lines with variable interdot separations (Figure 4A) offers support to this attractive possibility. Because of the apparent spillover effect[32] accompanying the assembly of the octadecanethiol features, dot-line no. 4 appears as a continuous wire despite being obtained from a monolayer template dot-line with dense but separate individual dots (not shown). However, a close examination of dot-lines nos. 3 and 4 after silver generation and solvent treatment (Figure 4E, phase image) reveals two rows of discrete particles, with only few coalesced particles in line no. 4. This clearly indicates that most silver particles in dot-line no. 4 were actually generated within separate template dots, the overlapping appearance of which being mainly caused by insufficient resolution of the SFM imaging rather than significant coalescence of adjacent octadecanethiol features. The solvent treatment results, as before (Figure 3), in a large height decrease of the imaged particles, from an average of ca. 7.5 (±0.7) nm to ca. 2.2 (±0.5) nm, and only a small relative decrease of their widths, from ca. 34 (±11) nm to ca. 27(±6) nm. Like before (Figure 3D) and contrary to the IR and UV−vis data (Figure 6, below), these thin platelike metal particles appear to be free of any organic coating. The final mild development with the SE solution adds, on the average, ca. 2 nm to both their heights and widths (measured across the dot-lines). This additional small growth is seen to produce the expected effect of closing most of the interdot gaps along dot-line no. 4, while the particles in dot-line no. 3 are still well separated from one another (Figure 4F).

Quantitative infrared and UV−vis spectral data were obtained from melt-assembled ultrathin films of eicosene (Figure 5) and octadecanethiol (Figure 6) on, respectively, large area silicon wafer substrates (ca. 3.5 cm × 2.0 cm) and fused quartz slides (4.0 cm × 1.0 cm) precoated with a well-defined carboxylic acid-terminated NTSox base monolayer.[33] The NTSox monolayer was derived from a highly ordered NTS precursor monolayer, by the in situ chemical oxidation of its top vinyl functions with organic permanganate ($KMnO_4$/crown ether complex in benzene).[11−15,34]

An inspection of the peak positions, relative intensities, and widths of the $-CH_2-$ stretch bands around 2917 and 2850 cm^{-1} in the IR (Si) and IR (quartz) spectra (Figures 5

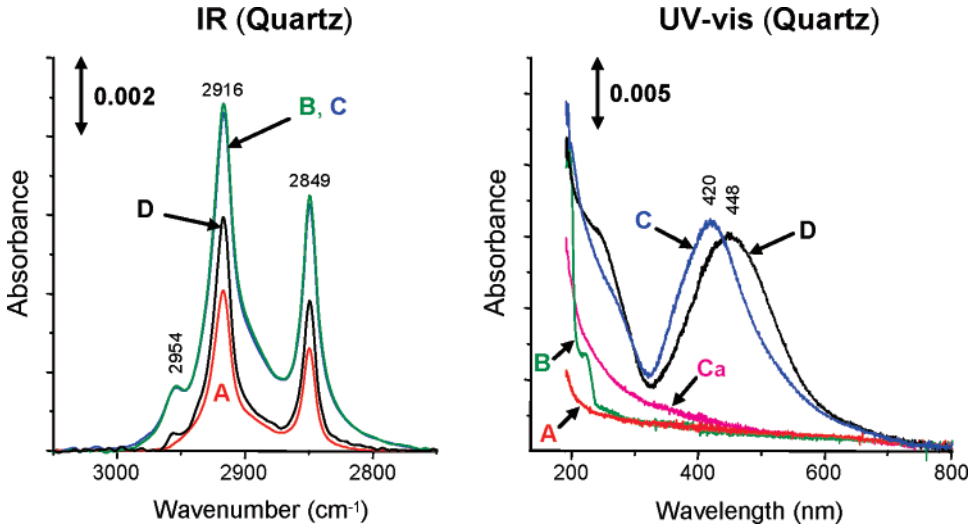

Figure 6. Quantitative FTIR and UV−visible spectra (transmission at normal incidence) recorded at consecutive steps during the preparation and subsequent chemical processing (as indicated in Figure 1) of a thin film of octadecanethiol assembled from melt on a base monolayer template with terminal −COOH functions produced on both sides of a fused quartz slide (NTSox/Q) (see text). (A) NTSox/Q base monolayer. (B) Octadecanethiol thin film assembled on the NTSox/Q base monolayer (B3 in Figure 1). (C) Metal−organic hybrid film resulting from the treatment of (B) for 10 min with an aqueous solution of $HAuCl_4$ (2.0×10^{-3} M) followed by brief exposure (~35 s) to the SE solution (C3 in Figure 1).[28] (D) same film after extraction of soluble organic material with diethyl ether (D in Figure 1). (Ca) UV−vis curve recorded after the treatment with $HAuCl_4$, before silver deposition from the SE solution. All curves represent net spectra of the respective film coatings after subtraction of the spectral contributions of the bare quartz substrate.

and 6, respectively) reveals that the molecular organization of both the eicosene and octadecanethiol films (ca. 4 and 1.2 monolayers thick, respectively)[33] resembles that of the corresponding NTSox base monolayers, the hydrocarbon tails of which were shown to adopt an essentially all-trans conformation, in a densely packed solidlike arrangement reminiscent of a rotator phase of long-chain *n*-alkanes.[15] It is further evident that both films are structurally stable under the conditions of the various chemical processing operations, only very little of the initial eicosene material being lost upon its oxidation to nonadecanoic acid.

The spectral region between 1900−700 cm^{-1} (Figure 5) provides direct evidence for: the quantitative conversion of eicosene to nonadecanoic acid (appearance, in curve C, of the hydrogen bonded −COOH band[15,34,35] at 1709 cm^{-1} and the concomitant disappearance of the $-CH{=}CH_2$ bands[14,15,34] at 1642 and 909 cm^{-1}, that are clearly visible in curve B); the quantitative conversion of the free nonadecanoic acid to its silver salt (disappearance, in curve D, of the 1709 cm^{-1} band and the concomitant appearance of characteristic silver carboxylate bands at 1517 and 1418 cm^{-1});[36] the reduction of the silver nonadecanoate to elemental silver with regeneration of the free nonadecanoic acid (reappearance, in curve E, of the −COOH band at 1710 cm^{-1} and the concomitant disappearance of the $-COO^-$ bands at 1517 and 1418 cm^{-1}); the quantitative dissolution of the free nonadecanoic acid in chloroform (disappearance of the 1710 cm^{-1} band in curve F, accompanied by a decrease of the peak absorbance at 2917 and 2850 cm^{-1} to ca. 28% of the corresponding values contributed by the overlayer film material in curves C,D,E). It is of interest to note that these transformations occur exclusively within the melt-assembled overlayer film, as conversion of the top carboxylic acid functions of the NTSox base monolayer to silver carboxylate demands significantly longer exposure times (at least 10 min) to the silver acetate reagent. This is obvious from the presence of the hydrogen bonded and monomeric −COOH bands of NTSox (around 1713 and 1733 cm^{-1}, respectively)[15,35] in all curves in which these are not masked by the much stronger −COOH band of the overlayer film, as well as that of the NTSox siloxane bands[14,15,34] around 1100 cm^{-1}, whose appearance in curves A and F is practically identical. Finally, the presence, in curve E, of a residual carboxylate band around 1540 cm^{-1} indicates that the regeneration of the free nonadecanoic acid upon the reduction of the Ag^+−nonadecanoate is not complete. The presence, in curves F, of a similar carboxylate band around 1556 cm^{-1}, together with the residual $-CH_2-$ bands around 2917 and 2850 cm^{-1}, may thus be ascribed to an insoluble Ag^+−nonadecanoate monolayer that covers the silver metal cores resulting from the reduction of the bulk Ag^+−nonadecanoate material.[37,38]

The UV−vis (quartz) spectra (Figure 6) offer direct evidence for the generation of elemental metal species in the process leading from the octadecanethiol film (curve B) to elemental silver nanoparticles displaying the characteristic plasmon band around 420 nm (curve C)[39] via the initial generation of tiny elemental gold clusters[28] that are below the critical particle size (~1.7 nm), giving rise to a distinct plasmon peak (curve Ca).[40] Taking into account the invariant contribution of the base NTSox monolayer, the residual IR peak absorbance at 2917 and 2850 cm^{-1} following the rinse with diethyl ether (curve D) corresponds to ca. 40% of the organic material present in the initial overlayer film (curves B,C). This is seen to induce only a minor red-shift in the position of the silver plasmon peak, together with a minor decrease of its intensity, which thus indicates that the metal

particles are not significantly affected by the removal of the soluble fraction of the organic film material.[41] These observations are consistent with the presence of an insoluble monolayer coating of silver thiolate covering the silver metal cores, similar to that of silver carboxylate discussed before. The discrepancy between these findings and the SFM data, which do not seem to be compatible with the presence of an insoluble monolayer coating on the silver nanoparticles generated within discrete template domains of nanoscale lateral dimensions remains to be clarified.

In conclusion, WDSA at the nanoscale was found to yield surprisingly stable surface-immobilized nanostructures, which points to the usefulness of this approach as a new tool of nanofabrication by chemical means. The present reported findings suggest interesting possibilities for confinement of diverse selected species, such as metal ions, metal and semiconductor nanoparticles, and organic compounds, in nanoreactors immobilized at predefined surface sites, within which various reaction sequences and reorganization processes may take place. In principle, any patterning technique capable of generating surface patterns that are sufficiently stable and display sufficient lyophilic/lyophobic contrast could be used to generate templates for WDSA.[22] Here we demonstrate the suitability of WDSA@CN as a generic chemical nanofabrication strategy that combines the nanoelectrochemical pattern inscription on a self-assembled base monolayer with various post-patterning chemical processing operations carried out at different hierarchical levels of complexity. The success of this approach depends on the judicious selection of materials and methods as well as on precise and careful application of the selected experimental protocols. For example, to achieve satisfactory selectivity in the immobilization and subsequent chemical processing of the desired species at the desired surface sites, it is necessary to use smooth and highly lyophobic (oleophobic as well as hydrophobic) surfaces, which implies assembling highly ordered, defect-free base monolayers. Using poor monolayers exhibiting low contact angles, large contact angle hysteresis, and limited structural stability will necessarily result in uncontrollable material adherence to defect sites, which may thus compromise the overall fabrication process. The specific experimental protocols described here serve to emphasize the conceptual and practical significance of WDSA@CN, and particularly its basic simplicity, wide scope, and synthetic flexibility, adaptable to the handling of diverse materials of interest. WDSA takes particular advantage of straightforward chemical modification protocols and inexpensive functional compounds that are commercially available. Exploiting physisorption rather than specific chemisorption, WDSA@CN is widely applicable, as a large variety of liquid or liquefiable materials (not necessarily amphiphilic) with appropriate wetting properties may in principle self-assemble via selective adherence at predefined sites of a chemically patterned monolayer.[22]

Acknowledgment. This research was supported by The Israel Science Foundation (grant no. 1109/04) and Minerva Foundation with funding from the Federal German Ministry of Education and Research. The NTS material was kindly supplied by Prof. Kazufumi Ogawa of Kagawa University, Takamatsu, Japan.

References

(1) Maoz, R.; Frydman, E.; Cohen, S. R.; Sagiv, J. *Adv. Mater.* **2000**, *12*, 725−731.
(2) Wouters, D.; Willems, R.; Hoeppener, S.; Flipse, C. F. J.; Schubert, U. S. *Adv. Funct. Mater.* **2005**, *15*, 938−944.
(3) Maoz, R.; Frydman, E.; Cohen, S. R.; Sagiv, J. *Adv. Mater.* **2000**, *12*, 424−429.
(4) Hoeppener, S.; Maoz, R.; Cohen, S. R.; Chi, L. F.; Fuchs, H.; Sagiv, J. *Adv. Mater.* **2002**, *14*, 1036−1041.
(5) Liu, S.; Maoz, R.; Schmid, G.; Sagiv, J. *Nano Lett.* **2002**, *2*, 1055−1060.
(6) Wouters, D.; Schubert, U. S. *Langmuir* **2003**, *19*, 9033−9038.
(7) Liu, S.; Maoz, R.; Sagiv, J. *Nano Lett.* **2004**, *4*, 845−851.
(8) Checco, A.; Cai, Y.; Gang, O.; Ocko, B. M. *Ultramicroscopy* **2006**, *106*, 703−708.
(9) Liu, S.; Maoz, R.; Sagiv, J. in preparation.
(10) Cohen, S. R.; Naaman, R.; Sagiv, J. *J. Phys. Chem.* **1986**, *90*, 3054−3056. Kluth, G. J.; Sung, M. M.; Maboudian, R. *Langmuir* **1997**, *13*, 3775−3780.
(11) Maoz, R.; Sagiv, J. *Thin Solid Films* **1985**, *132*, 135−151.
(12) Maoz, R.; Cohen, H.; Sagiv, J. *Langmuir* **1998**, *14*, 5988−5993.
(13) Maoz, R.; Yam, R.; Berkovic, G.; Sagiv, J. In *Thin Films*; Ulman A., Ed.; Academic Press: San Diego, 1995; Vol. 20, pp 41−68.
(14) Maoz, R.; Matlis, S.; DiMasi, E.; Ocko, B. M.; Sagiv, J. *Nature* **1996**, *384*, 150−153. Maoz, R.; Sagiv, J. *Adv. Mater.* **1998**, *10*, 580−584.
(15) Maoz, R.; Sagiv, J.; Degenhardt, D.; Möhwald, H.; Quint, P. *Supramol. Sci.* **1995**, *2*, 9−24.
(16) Baptiste, A.; Gibaud, A.; Bardeau, J. F.; Wen, K.; Maoz, R.; Sagiv, J.; Ocko, B. M. *Langmuir* **2002**, *18*, 3916−3922.
(17) Onclin, S.; Ravoo, B. J.; Reinhoudt, D. N. *Angew. Chem., Int. Ed.* **2005**, *44*, 6282−6304.
(18) Netzer, L.; Iscovici, R.; Sagiv, J. *Thin Solid Films* **1983**, *99*, 235−241.
(19) Barness, Y.; Gershevitz, O.; Sekar, M.; Sukenik, C. N. *Langmuir* **2000**, *16*, 247−251.
(20) Li, X.-M.; Péter, M.; Huskens, J.; Reinhoudt, D. N. *Nano Lett.* **2003**, *3*, 1449−1453.
(21) Huang, N-P.; Michel, R.; Voros, J.; Textor, M.; Hofer, R.; Rossi, A.; Elbert, D. L.; Hubbell, J. A.; Spencer, N. D. *Langmuir* **2001**, *17*, 489−498.
(22) The methods applicable to the investigation of nanopatterned materials are limited because of the inherent small dimensions of such systems. Therefore, studies of matter behavior at the nanoscale need to be complemented by extrapolations deriving from the study of analogous systems at variable length scales beyond the nanoscale. We have thus examined the WDSA of a number of different materials on variable lateral length scales from nanometer to centimeter, which allowed us to combine SFM imaging with methods such as quantitative micro-FTIR spectroscopy, optical microscopy, and direct contact angle measurements. Monolayer patterns suitable for WDSA with characteristic dimensions in the range micrometer−centimeter were generated by combining OTS photodesorption with the self-assembly, in the depleted surface regions, of an NTS monolayer and its subsequent in situ modification, leading to the desired polar surface functions (Chowdhury, D.; Maoz, R.; Cohen, S. R.; Sagiv, J., in preparation).
(23) While preparing this material for publication, we came across the important work of S. M. Troian et al. devoted to some of the basic aspects of the dip-coating of micropatterned surfaces with wettable features spanning lateral dimensions in the micrometer−millimeter range.[24,25]
(24) Darhuber, A. A.; Troian, S. M.; Miller, S. M.; Wagner, S. *J. Appl. Phys.* **2000**, *87*, 7768−7775.
(25) Darhuber, A. A.; Troian, S. M.; Davis, J. M.; Miller, S. M.; Wagner, S. *J. Appl. Phys.* **2000**, *88*, 5119−5126.
(26) Wen, K. Ph. D. Thesis. Weizmann Institute of Science, April, 1999.
(27) Frydman, E. Ph. D. Thesis.Weizmann Institute of Science, September, 1999.
(28) Contrary to what was initially believed,[1] it has later been found that silver deposition in this process is catalyzed by tiny gold nanoclusters produced upon the spontaneous reduction, by the thiol itself, of Au^{3+} to elemental gold (Berson, J.; Maoz, R.; Cohen, H.; Sagiv, J., to be published).

(29) Patterns were written with bias voltages in the range 8−17 V, depending on the performance of each probe as determined experimentally before its use in a particular patterning experiment.
(30) Schollmeyer, H.; Struth, B.; Riegler, H. *Langmuir* **2003**, *19*, 5042−5051. Lazar, P.; Schollmeyer, H.; Riegler, H. *Phys. Rev. Lett.* **2005**, *94*, 116101-1−116101-4.
(31) The heights of surface features obtained in the WDSA process scale in a rather complex manner with their lateral dimensions.[22,24,25] We found that several different materials assembled from the melt on monolayer nanopatterns with similar lateral dimensions yield features with similar nanometric heights. These include 3-chlorophenol and gallium, which are not long-tail hydrocarbon compounds. In view of these observations and the limited set of experimental data presently available, the suggested molecular organization of eicosene nanodomains remains at this stage tentative.
(32) Rauscher, M.; Popescu, M. N.; Dietrich, S. *J. Phys.: Condens. Matter* **2005**, *17*, S577−S593.
(33) Eicosene or octadecanethiol films assembled by retraction from melt on large area lyophilic surfaces have micrometric thickness.[22] To produce such films with thicknesses comparable with those of melt-assembled nanoscale features of these compounds, we used Scotch tape peeling to remove material from initially obtained micrometric films, until a final thickness of not more than several monolayers (as indicated by the infrared band intensities) was reached.
(34) Maoz, R.; Cohen, S. R.; Sagiv, J. *Adv. Mater.* **1999**, *11*, 55−61.
(35) Nuzzo, R.; Dubois, L. H.; Allara, D. L. *J. Am. Chem. Soc.* **1990**, *112*, 558−569.
(36) Lee, S. J.; Han, S. W.; Choi, H. J.; Kim, K. *J. Phys. Chem. B* **2002**, *106*, 2892−2900. Lee, S. J.; Kim, K. *Vib. Spectrosc.* **1998**, *18*, 187−201.
(37) The variable peak position of this broad carboxylate band is indicative of different binding modes of the carboxylate to different local sites on the silver cores (see Merklin, G. T.; Griffiths, P. R. *J. Phys. Chem. B* **1997**, *101*, 5810−5813. Mehrotra, R. C.; Bohra, R. *Metal Carboxylates;* Academic Press: London, 1983).
(38) It is of interest to note that no enhancement of the infrared absorption could be detected in the present film samples following the generation of silver particles, contrary to what was observed in organic films in contact with evaporated silver island films (see, for example: Kamata, T.: Kato, A; Umemura, J.; Takenaka, T. *Langmuir* **1987**, *3*, 1150−1154).
(39) See, for example: Schimmel, T.; Bingler, H.-G.; Franzke, D.; Wokaun, A. *Adv. Mater.* **1994**, *6*, 303−307.
(40) Alvarez, M. M.; Khoury, J. T.; Schaaff, T. G.; Shafigullin, M. N.; Vezmar, I.; Whetten, R. L. *J. Phys. Chem. B* **1997**, *101*, 3706−3712. Warner, M. G.; Reed, S. M.; Hutchison, J. E. *Chem. Mater.* **2000**, *12*, 3316−3320. Wuelfing, W. P.; Zamborini, F. P.; Tempelton, A. C.; Wen, X.; Yoon, H.; Murray, R. W. *Chem. Mater.* **2001**, *13*, 87−95.
(41) Kalyuzhny, G.; Vaskevich, A.; Schneeweiss, M. A; Rubinstein, I. *Chem.—Eur. J.* **2002**, *8*, 3850−3857.

NL070842X